2003

Apparent break in earthquake scaling due to path and site effects on deep borehole recordings

Satoshi Ide
University of Tokyo

Gregory C. Beroza
Stanford University

Stephanie G. Prejean
U.S. Geological Survey

William L. Ellsworth
U.S. Geological Survey

Apparent break in earthquake scaling due to path and site effects on deep borehole recordings

Satoshi Ide
Department of Earth and Planetary Science, University of Tokyo, Tokyo, Japan

Gregory C. Beroza
Department of Geophysics, Stanford University, Stanford, California, USA

Stephanie G. Prejean and William L. Ellsworth
U.S. Geological Survey, Menlo Park, California, USA

Received 31 October 2001; revised 7 January 2003; accepted 11 February 2003; published 24 May 2003.

[1] We reexamine the scaling of stress drop and apparent stress, rigidity times the ratio between seismically radiated energy to seismic moment, with earthquake size for a set of microearthquakes recorded in a deep borehole in Long Valley, California. In the first set of calculations, we assume a constant Q and solve for the corner frequency and seismic moment. In the second set of calculations, we model the spectral ratio of nearby events to determine the same quantities. We find that the spectral ratio technique, which can account for path and site effects or nonconstant Q, yields higher stress drops, particularly for the smaller events in the data set. The measurements determined from spectral ratios indicate no departure from constant stress drop scaling down to the smallest events in our data set (M_w 0.8). Our results indicate that propagation effects can contaminate measurements of source parameters even in the relatively clean recording environment of a deep borehole, just as they do at the Earth's surface. The scaling of source properties of microearthquakes made from deep borehole recordings may need to be reevaluated. *INDEX TERMS:* 7203 Seismology: Body wave propagation; 7205 Seismology: Continental crust (1242); 7215 Seismology: Earthquake parameters; *KEYWORDS:* seismic energy, apparent stress, scaling, borehole, Long Valley, artifact

Citation: Ide, S., G. C. Beroza, S. G. Prejean, and W. L. Ellsworth, Apparent break in earthquake scaling due to path and site effects on deep borehole recordings, *J. Geophys. Res.*, *108*(B5), 2271, doi:10.1029/2001JB001617, 2003.

1. Introduction

[2] For earthquakes above M_w 3, it has long been known that stress drop does not vary systematically with earthquake size. This results in well-known scaling relationships of characteristic length and time with seismic moment [e.g., *Kanamori and Anderson*, 1975; *Hanks*, 1977]. Several studies have suggested that the scaling of small earthquakes is different from that of larger events. *Archuleta et al.* [1982] and *Archuleta* [1986] analyzed surface and shallow borehole records of earthquakes in the Mammoth Lakes, California and found that the stress drop decreases with decreasing moment for events smaller than M 3. Using deep borehole recordings at 2.5-km depth in the Cajon Pass, California, *Abercrombie* [1995] concluded that there is no such breakdown in constant stress drop scaling. From the same analysis, however, she also concluded that the apparent stress (rigidity times the ratio between seismically radiated energy to seismic moment) decreases with decreasing seismic moment. More recently, *Prejean and Ellsworth* [2001] used data from a 2-km-deep borehole in Long Valley caldera, California, to determine the stress drop and apparent stress of earthquakes from M_w 0.5 to 5.0 and reached similar conclusions.

[3] There are many estimates of apparent stress and the energy/moment ratio across a wide range of earthquake size. Although these estimates seem to have a common upper limit defined by the average shear stress level [*McGarr*, 1999], there are often size dependencies within individual data sets [*Gibowicz et al.*, 1991; *Kanamori et al.*, 1993; *Abercrombie*, 1995; *Mayeda and Walter*, 1996; *Jost et al.*, 1998; *Prejean and Ellsworth*, 2001] such that changes in scaling within each study are more rapid than the scaling changes across studies. Recording bandwidth limitations can severely affect the estimate of seismic energy [*Boore*, 1986; *Di Bona and Rovelli*, 1988; *Singh and Ordaz*, 1994; *Hough*, 1996], and *Ide and Beroza* [2001] have shown that most of the observed size dependence can be attributed to artifacts arising from bandwidth limitations. The artifacts they cite are (1) substantial missing contributions from waves with frequencies well above the corner frequency [e.g., *Gibowicz et al.*, 1991; *Jost et al.*, 1998] and (2) event selection with a constant upper cutoff on the corner fre-

0148-0227/03/2001JB001617$09.00

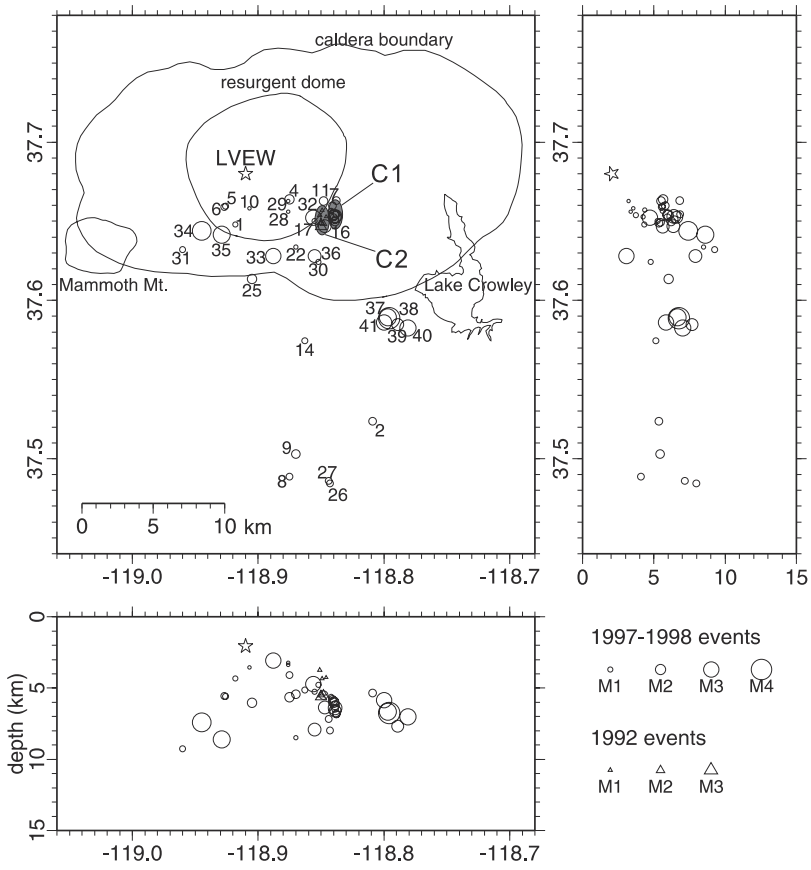

Figure 1. Map of studied earthquakes and seismometer locations with cross sections. Long Valley caldera and resurgent dome boundaries are also shown. Events that occurred in 1997–1998 and were studied by *Prejean and Ellsworth* [2001] are shown by circles, while events in 1992 are shown by triangles. The number shows the earthquake ID from Table 1. For clusters C1 and C2, only the approximate area of clusters is shown. Star represents the location of seismometer.

quency, which will bias event selection to lower stress drop events for smaller earthquakes in the sample [e.g., *Abercrombie*, 1995; *Mayeda and Walter*, 1996]. Even when these sources of bias are accounted for, however, there remains a size dependency that cannot be explained by either of these mechanisms in the results of *Abercrombie* [1995] and *Prejean and Ellsworth* [2001].

[4] Both of these studies modeled crustal attenuation with a frequency independent Q operator. They also did not account for the possibility of frequency-dependent path or site effects in the data, both of which are thought to be reasonable assumptions given the extremely broad band nature of borehole recordings and the clean, pulse-like nature of seismograms recorded in borehole environments. The validity of this assumption is to some extent untested, however, even in deep boreholes where seismic noise and path effects are clearly greatly reduced as compared to surface recordings [*Abercrombie*, 1998].

[5] If colocated events are available, it is possible to cancel path and site effects by taking the spectral amplitude ratio between the spectra of the two events [e.g., *Berckhemer*, 1962; *Bakun and Bufe*, 1975; *Mueller*, 1985]. *Hough* [1997] proved the effectiveness of this approach and *Hough et al.* [1999] called it the multiple empirical Green function (MEGF) method. They used it to analyze the attenuation structure and source properties of small earthquakes ($-0.4 < M < 1.3$) at the Coso Geothermal area, California.

[6] In this study, we reexamine the data of *Prejean and Ellsworth* [2001] and additional data in the same area. We compare results from constant Q analysis and MEGF analysis to test whether the assumption of constant Q and negligible path and site effects for borehole recordings might affect estimates of source properties.

2. Constant Q Analysis

[7] Figure 1 and Table 1 show the locations of the seismometer and the events analyzed by *Prejean and Ellsworth* [2001]. The event locations are relocated using the double difference earthquake location algorithm of *Waldhauser and Ellsworth* [2000]. The seismometer is located at 2054 m depth in the Long Valley Exploratory Well. At this level, the well deviates from vertical by only two degrees. The sensor is a three-component geophone with a pendulum frequency of 10 Hz and damping constant of 0.7. Events are recorded at three different sampling rates: 1000 (event 1–31), 250 (32–35), and 10,000 (36–41) sps. The data at frequencies higher than about 200 Hz show an unusual attenuation of the vertical component, so we limit our analysis to frequencies below 180 Hz.

Table 1. Earthquake Analyzed

ID	Time[a]	Latitude, °N	Longitude, °W	Depth, km	M_w	Group
01	972541854	37.6480	118.9177	4.34	1.1	–
02	972542323	37.5237	118.8088	5.33	1.5	–
03	972561934	37.6630	118.8384	6.80	1.6	C1
04	972582242	37.6639	118.8753	5.63	1.8	–
05	972590251	37.6595	118.9259	5.57	1.3	–
06	972590912	37.6591	118.9267	5.56	1.3	–
07	972600247	37.6597	118.8415	5.79	1.6	–
08	972602200	37.4888	118.8747	4.10	1.3	–
09	972631047	37.5030	118.8695	5.44	1.7	–
10	972640331	37.6582	118.9075	3.55	0.7	–
11	972640949	37.6628	118.8476	5.49	1.7	–
12	972641614	37.6470	118.8465	6.35	2.5	C1
13	972641620	37.6565	118.8417	5.60	1.1	C1
14	972641659	37.5745	118.8628	5.15	1.1	–
15	972641856	37.6525	118.8390	6.59	2.2	C1
16	972641910	37.6511	118.8391	6.46	1.3	–
17	972641915	37.6502	118.8552	5.25	1.0	–
18	972642050	37.6531	118.8387	6.40	2.7	C1
19	972642102	37.6542	118.8404	5.95	1.7	C1
20	972642107	37.6540	118.8401	6.00	2.0	C1
21	972642115	37.6525	118.8401	5.94	1.3	C1
22	972642301	37.6337	118.8701	8.47	0.7	–
23	972642340	37.6544	118.8380	6.85	1.4	C1
24	972650213	37.6498	118.8394	6.20	1.7	C1
25	972660130	37.6134	118.9052	6.02	1.8	–
26	972660256	37.4845	118.8432	7.98	1.3	–
27	972660326	37.4860	118.8440	7.18	1.4	–
28	972660631	37.6561	118.8757	3.37	0.7	–
29	972660734	37.6629	118.8763	3.22	0.6	–
30	972670150	37.6243	118.8520	4.77	1.0	–
31	972670911	37.6320	118.9597	9.25	1.2	–
32	973081302	37.6522	118.8558	4.73	2.9	–
33	973111517	37.6280	118.8885	3.08	3.0	–
34	973570219	37.6440	118.9446	7.40	3.5	–
35	980381938	37.6415	118.9290	8.61	3.5	–
36	981440310	37.6280	118.8553	7.93	2.4	–
37	981590355	37.5893	118.7975	6.66	3.1	–
38	981600524	37.5887	118.7955	6.75	5.0[b]	–
39	981600829	37.5848	118.7887	7.67	2.5	–
40	981600845	37.5825	118.7813	7.02	3.1	–
41	981601330	37.5862	118.8002	5.85	3.2	–
A1	923130825	37.6467	118.8505	5.61	2.3	C2
A2	923130842	37.6528	118.8458	4.25	0.7	C2
A3	923130902	37.6487	118.8480	5.35	1.2	C2
A4	923131038	37.6538	118.8512	3.74	1.0	C2
A5	923131735	37.6492	118.8500	5.47	1.4	C2

[a]Year, Julian day, hour, and minute.
[b]Taken from *Prejean and Ellsworth* [2001].

[8] In this paper, we also analyzed a small cluster of five earthquakes that occurred in 1992 (Table 1 and Figure 1). These events were recorded by a three-component set of very broad band Wilcoxon piezeoelectric accelerometers (0.05–200 Hz) in the same borehole. The depth of the instrument is almost the same (2046 m) as in the case of the 1997 data. The sampling rate is 500 Hz for these data.

[9] We first rotate the three component velocity seismograms to *P* (radial), *SH* (transverse), and *SV* wave directions, minimizing *SH* and *SV* wave energies before the *S* arrival. Then, using *P* and *S* wave windows of fixed lengths, we calculate the Fourier spectral amplitude for each wave. The window lengths are 0.4 s and 0.6 s for *P* and *S* waves, starting from *P* and *S* arrivals, respectively. The length of the window can be a possible source of uncertainty because the length determines how much of the coda waves are included in the energy estimation. However, as we show in Appendix A, the effect of coda waves is not significant in this analysis and various lengths of time window give almost identical results for this data set.

[10] After correcting instrumental response, we resample each spectral amplitude at equal intervals in log frequency at $\Delta \log f = 0.05$ and take a moving window average of length $\Delta \log f = 0.3$. By averaging we are able to estimate the standard deviation of the spectrum. The *S* wave amplitude spectrum is calculated as the vector summation of *SH* and *SV* spectra. Noise spectra are calculated using the same scheme on the same length of presignal record. We adjust the standard deviation based on the signal-to-noise ratio. However, for data taken at 10,000 sps sampling rate the presignal length is too short to characterize the noise, and we made no adjustment for these data.

[11] In this study we used a spectral inversion method to estimate source parameters and a constant attenuation parameter. Our approach is similar to the method of *Masuda and Suzuki* [1982] and *Anderson and Humphrey* [1991]. We assume a simple omega square spectrum [*Aki*, 1967; *Brune*, 1970]. Following *Boatwright* [1978], we approximate the velocity amplitude spectrum as

$$|\dot{u}^c(f)| \approx \frac{R^c}{2\rho(v^c)^3 r} \frac{fM_o}{\left(1 + \left(f/f_c^c\right)^4\right)^{1/2}} \exp\left(-\frac{\pi f t^c}{Q^c}\right), \quad (1)$$

where R^c, v^c, f_c^c, t^c, and Q^c are radiation pattern, wave velocity, corner frequency, travel time, and attenuation coefficients of wave type c (superscript), which may be either a *P* or *S* wave, and ρ, *r*, and M_o are density, hypocentral distance, and seismic moment, respectively. In this paper, we used $v^P = 5.8$ km/s, $v^S = 3.3$ km/s, $\rho = 2700$ kg/m^3. The hypocentral distances and travel times are measured from the *S-P* time and these velocity values. For the radiation pattern, we used average values $R^P = 2/\sqrt{15}, R^S = \sqrt{2/5}$ [*Aki and Richards*, 1980].

[12] Taking the logarithm of this equation,

$$\log \dot{u}^c(f) \approx g\left(f; \log M_o, 1/Q^c, f_c^c\right) \quad (2)$$

$$g\left(f; \log M_o, 1/Q^c, f_c^c\right) = \log\left(\frac{R^c f}{2\rho(v^c)^3 r}\right) + \log M_o - \frac{1}{2}\log\left(1 + \left(f/f_c^c\right)^4\right) - \frac{\pi f t^c}{Q^c}\log e. \quad (3)$$

The equations for the sampled frequencies comprise a linear inverse problem for M_o and $1/Q^c$ when f_c^c is fixed. We solve this problem for each f_c^c, and find f_c^c by a grid search that minimizes the residual

$$Res = \sum_i \frac{\left[\log \dot{u}^c(f_i) - g\left(f_i; \log M_o, 1/Q^c, f_c^c\right)\right]^2}{\sigma_i^2}, \quad (4)$$

where σ_i is the standard deviation for each data point computed when we resampled the spectrum.

[13] Figure 2 shows examples of observed spectra and fitted omega square and constant *Q* model, together with the

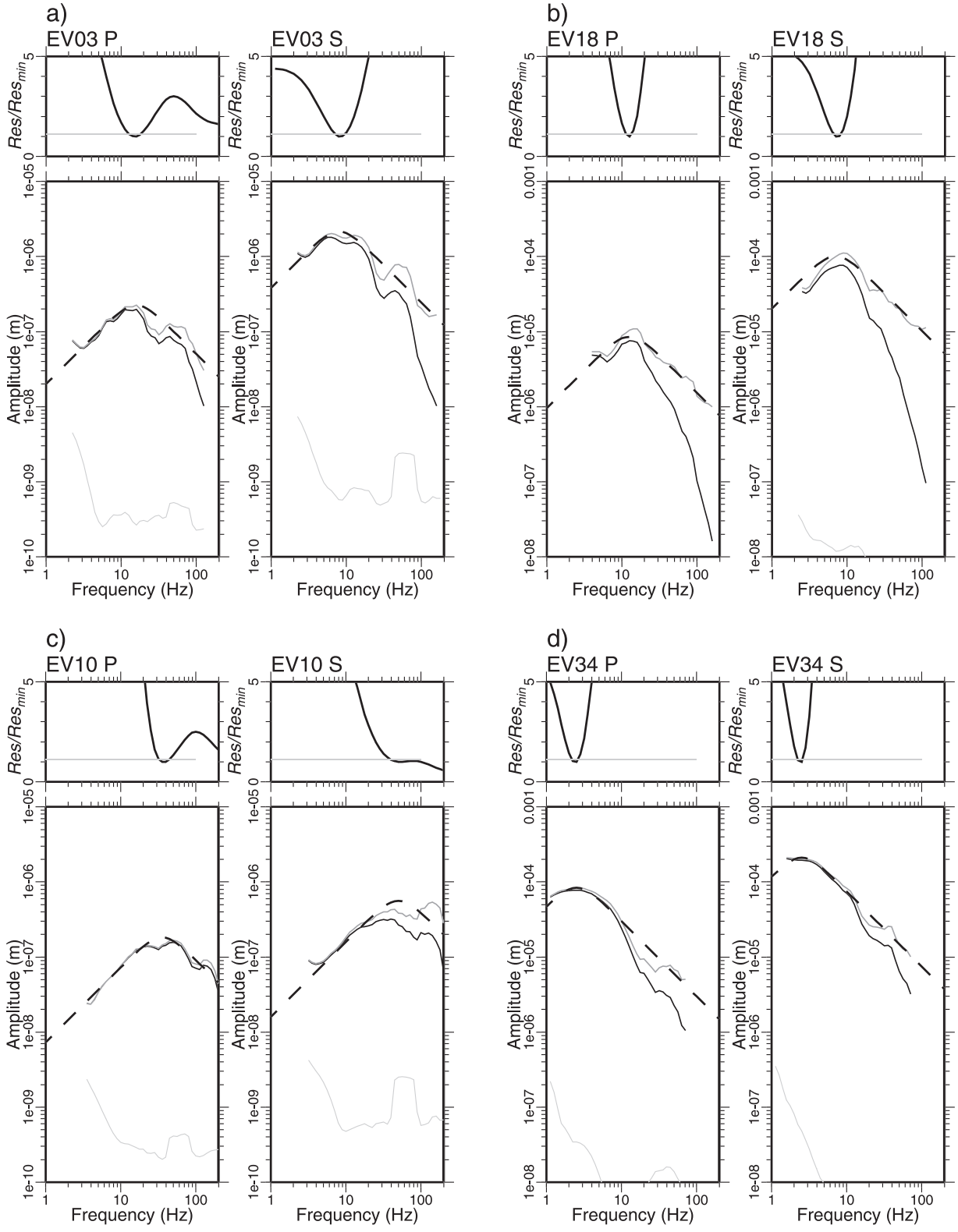

Figure 2. Example of spectra and fitting result with the constant Q assumption. For P or S wave. (top) Residual curve and (bottom) original spectrum (black solid line), Q corrected spectrum (dark gray line), noise spectrum (light gray line), and fitted omega square model (dashed line).

Table 2. Source Parameter Determined Assuming Constant Q

ID	M_o^P, N m	M_o^S, N m	f_c^P, Hz	f_c^S, Hz	Q^P	Q^S	E^P [f_1], J [Hz]	E^S [f_1], J [Hz]	$\Delta\sigma_B$, MPa	σ_a, MPa
01	4.41e + 10	7.26e + 10	158	25	99	242	7.11e + 05 [281]	1.31e + 05 [281]	0.22	0.42
02	2.26e + 11	2.44e + 11	15	12	1096	582	2.21e + 04 [177]	2.93e + 05 [177]	0.096	0.039
03	1.41e + 11	5.00e + 11	15	7.9	447	389	3.80e + 04 [141]	1.49e + 05 [177]	0.037	0.017
04	2.56e + 11	9.15e + 11	223	31	101	203	6.53e + 07 [223]	2.98e + 07 [281]	4.1	4.8
05	1.31e + 11	9.01e + 10	28	25	276	293	2.61e + 04 [281]	4.16e + 05 [281]	0.41	0.12
06	1.49e + 11	7.41e + 10	19	22	302	319	8.73e + 03 [281]	3.36e + 05 [281]	0.28	0.091
07	2.56e + 11	3.00e + 11	28	22	166	195	1.66e + 05 [199]	2.26e + 06 [177]	0.70	0.26
08	8.90e + 10	1.63e + 11	44	17	355	581	1.11e + 05 [158]	2.72e + 05 [199]	0.15	0.089
09	8.42e + 10	7.05e + 11	63	15	338	586	4.56e + 06 [199]	1.98e + 06 [177]	0.31	0.49
10	2.20e + 10	8.86e + 09	35	50	1311	407	1.04e + 03 [281]	8.98e + 04 [281]	0.46	0.17
11	3.33e + 11	5.90e + 11	35	15	122	184	8.73e + 05 [199]	2.25e + 06 [177]	0.37	0.20
12	9.11e + 12	4.25e + 12	10	12	169	230	4.21e + 06 [199]	2.35e + 08 [177]	2.7	1.1
13	4.76e + 10	5.33e + 10	25	15	339	477	4.04e + 03 [199]	2.46e + 04 [199]	0.040	0.017
14	5.14e + 10	6.27e + 10	35	17	526	677	1.35e + 04 [199]	4.49e + 04 [223]	0.066	0.030
15	1.16e + 12	4.01e + 12	15	7.9	244	232	3.38e + 06 [199]	9.44e + 06 [158]	0.30	0.15
16	5.59e + 10	1.47e + 11	39	15	260	332	6.16e + 04 [199]	1.15e + 05 [223]	0.081	0.051
17	2.97e + 10	5.35e + 10	39	35	791	263	1.08e + 04 [281]	1.97e + 05 [281]	0.42	0.15
18	6.69e + 12	2.60e + 13	12	7.1	147	158	6.46e + 07 [177]	2.50e + 08 [125]	1.4	0.57
19	4.15e + 11	6.43e + 11	28	22	178	178	6.92e + 05 [199]	8.84e + 06 [177]	1.3	0.53
20	1.00e + 12	1.83e + 12	19	12	179	210	1.81e + 06 [141]	1.15e + 07 [158]	0.58	0.28
21	6.63e + 10	1.50e + 11	39	17	250	296	7.47e + 04 [199]	1.78e + 05 [199]	0.13	0.069
22	4.76e + 09	2.51e + 10	50	25	Inf	895	2.60e + 03 [251]	1.02e + 04 [199]	0.055	0.025
23	1.61e + 11	1.57e + 11	31	25	194	255	7.89e + 04 [199]	1.11e + 06 [223]	0.59	0.22
24	2.82e + 11	4.95e + 11	35	17	212	257	7.63e + 05 [223]	2.94e + 06 [199]	0.45	0.28
25	5.32e + 11	8.13e + 11	39	25	168	233	2.68e + 06 [251]	2.28e + 07 [199]	2.5	1.1
26	1.43e + 11	7.61e + 10	15	35	867	488	4.15e + 03 [177]	2.86e + 06 [177]	1.1	0.77
27	2.55e + 11	6.60e + 10	281	35	209	530	1.34e + 07 [281]	5.00e + 06 [177]	1.6	3.4
28	1.04e + 10	1.83e + 10	89	56	211	249	1.03e + 04 [281]	1.10e + 05 [251]	0.60	0.25
29	1.07e + 10	6.96e + 09	35	22	200	214	3.14e + 02 [199]	2.57e + 03 [199]	0.022	0.010
30	4.54e + 10	2.40e + 10	39	44	2212	347	6.93e + 03 [177]	2.53e + 05 [251]	0.70	0.22
31	9.05e + 10	5.81e + 10	12	10	497	1178	1.07e + 03 [158]	1.34e + 04 [199]	0.018	0.006
32	2.29e + 13	4.23e + 13	7.9	5.6	928	523	5.15e + 07 [70]	4.54e + 08 [70]	1.4	0.46
33	6.63e + 13	9.43e + 12	7.1	12	133	161	4.76e + 07 [70]	7.13e + 09 [70]	15.5	5.6
34	3.02e + 14	1.39e + 14	2.5	2.5	158	382	8.80e + 07 [70]	2.03e + 09 [70]	0.81	0.28
35	3.07e + 14	9.92e + 13	2.2	2.8	Inf	2941	4.85e + 07 [70]	2.43e + 09 [70]	1.1	0.36
36	4.13e + 12	6.70e + 12	15	14	275	356	1.14e + 07 [223]	2.63e + 08 [223]	3.5	1.5
37	8.27e + 13	2.98e + 13	8.9	8.9	219	292	2.25e + 08 [70]	5.56e + 09 [70]	9.4	3.0
38	8.03e + 13	3.31e + 14	12	4.5	322	413	8.97e + 09 [199]	1.12e + 10 [141]	4.4	2.9
39	9.35e + 12	5.49e + 12	4.0	6.3	660	467	3.17e + 05 [177]	3.12e + 07 [177]	0.44	0.12
40	7.02e + 13	5.04e + 13	7.1	6.3	343	355	2.01e + 08 [177]	3.14e + 09 [125]	3.6	1.6
41	1.27e + 14	1.05e + 13	6.3	14	297	316	1.10e + 08 [199]	5.04e + 10 [125]	44.6	21.6
A1	3.35e + 12	3.00e + 12	17	12	119	189	6.51e + 06 [112]	4.99e + 07 [89]	1.3	0.52
A2	1.29e + 10	1.55e + 10	50	70	240	161	2.01e + 03 [141]	1.22e + 05 [141]	1.2	0.26
A3	7.88e + 10	8.81e + 10	50	14	138	4804	7.22e + 04 [141]	4.61e + 04 [100]	0.054	0.042
A4	5.81e + 10	2.35e + 10	31	89	360	170	4.83e + 03 [141]	8.98e + 05 [100]	6.8	0.65
A5	1.39e + 11	1.30e + 11	19	14	224	310	1.35e + 04 [112]	1.24e + 05 [141]	0.087	0.030

residual from equation (4). For some events, the minimum appeared at the edge of search area (Figure 2c). In these cases, we did not take that minimum and instead took the second minimum as the best estimate. Because of bandwidth limitations, some events have small residuals over a wide range of frequencies, suggesting that a reliable estimate of the corner frequency is difficult to define for these spectra (Figure 2c). Although the result is stable even for large events (Figure 2d), for the largest event (EV38) we could not obtain a reasonable solution, because the main frequency band of this event is far lower than the natural frequency of seismometer (10 Hz). Therefore we did not analyze this event further. To estimate the range of possible corner frequencies, we chose the upper and lower limits at which the residual increases to four times of data variance,

$$\sigma_d = Res/(N-3), \tag{5}$$

where N is the number of data points. This range corresponds approximately to twice the standard deviation of the corner frequency. The possible ranges for seismic moment and Q are estimated in the same manner. The spectrum of 40 events appear to be well explained by an omega square curve with a constant Q.

[14] Table 2 summarizes the estimated parameters. In Table 2, we also show radiated energy estimates for each spectrum. It is calculated using [*Boatwright and Fletcher*, 1984]

$$E^c = 4\pi\rho v^c r^2 \times 2\int_{f_0}^{f_1} \left| \dot{u}^c(f) \exp\left(\frac{\pi f t^c}{Q^c}\right)\right|^2 df; \tag{6}$$

f_0 and f_1 are the lower and upper limits of integration. The upper limits are shown in Table 2.

[15] Usually the estimates of seismic moment from P and S, M_o^P and M_o^S respectively, are found to be slightly different. We calculate the average seismic moment, $\bar{M}_o$, as

$$\bar{M}_o = \left(M_o^P + M_o^S\right)/2. \tag{7}$$

Energy values are calculated using amplitude spectra whose lower limit is adjusted to this average seismic moment value and can be written

$$\bar{E}^c = \left(\frac{\bar{M}_o}{M_o^c}\right)^2 E^c. \quad (8)$$

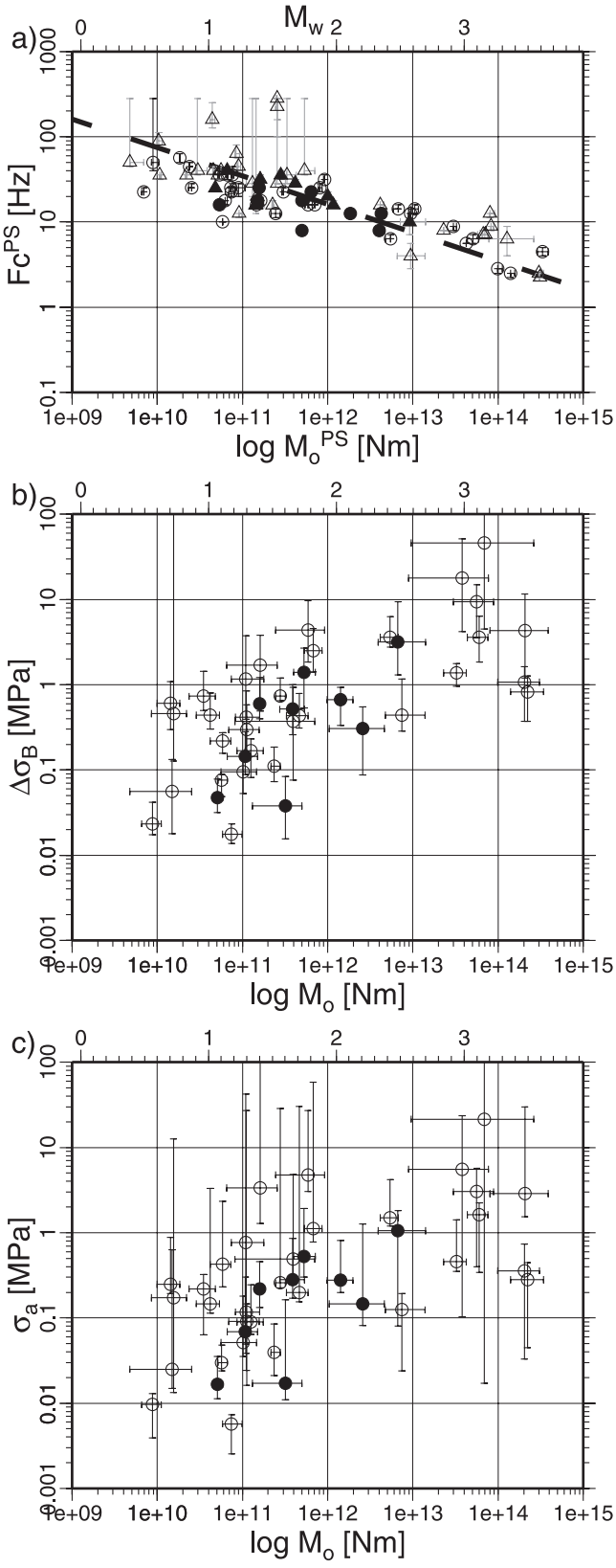

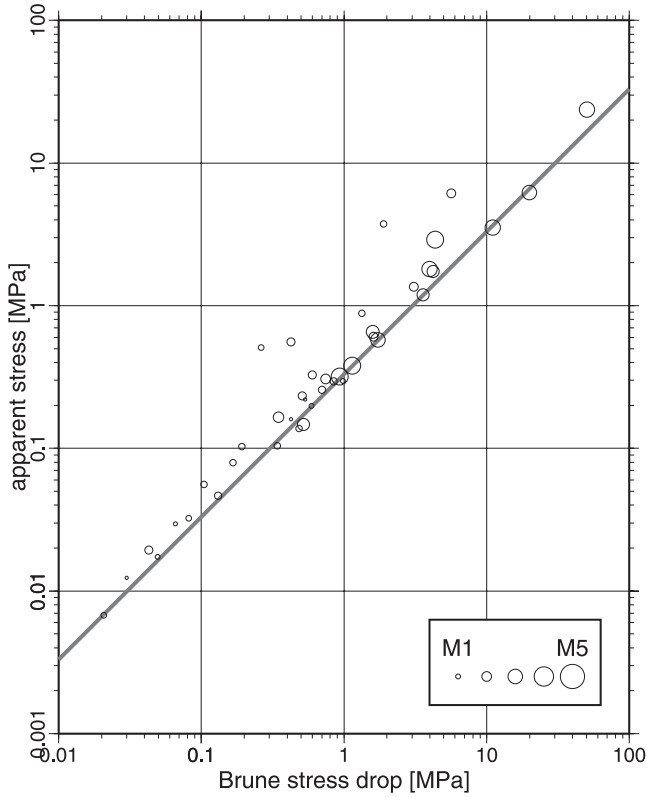

Figure 4. Comparison between Brune stress drop and apparent stress determined by constant Q analysis. Solid line shows the relation of $\sigma_a = 0.33\ \Delta\sigma_B$, the theoretical relationship between Brune stress drop and apparent stress for *Boatwright* [1978] ω^2 model.

[16] Brune stress drop [*Brune*, 1970] $\Delta\sigma_B$ and apparent stress [*Wyss and Brune*, 1968] σ_a are calculated using

$$\Delta\sigma_B = \frac{7}{16}\bar{M}_o\left(\frac{2\pi f_c^S}{2.34v^S}\right)^3 \quad (9)$$

$$\sigma_a = \mu\frac{\bar{E}^P + \bar{E}^S}{\bar{M}_o}, \quad (10)$$

where μ is the rigidity. In this expression, we include correction of seismic moment to account for radiation pattern difference. These values are also shown in Table 2.

[17] Figure 3 shows the relationship between seismic moment and corner frequency f_c, Brune stress drop $\Delta\sigma_B$, and apparent stress σ_a, respectively, together with the

Figure 3. (opposite) Scaling relation from constant Q analysis. (a) Seismic moment versus corner frequency. Triangle and circle represent the value determined for each P or S wave with error bar. Dashed line corresponds to constant stress drop of 1 MPa. (b) Comparison between seismic moment and Brune stress drop. (c) Comparison between seismic moment and apparent stress. In all plots, events that belong to cluster C1 are shown by solid symbols, while others are shown by open symbols.

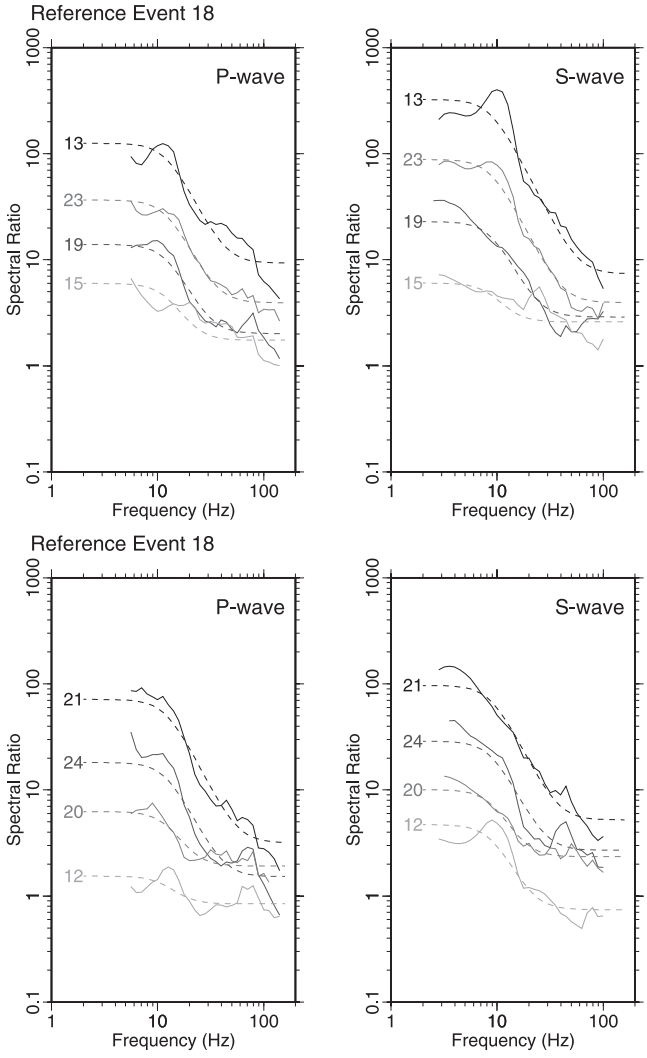

Figure 5. Example of spectral ratio (solid line) and fitting curve for the theoretical spectral ratio assuming an omega square model (dashed line). Each curve is the spectral ratio relative to event 18, the largest event in C1.

possible range of their values. The uncertainties of corner frequency and seismic moment are reflected in the large error bars. Considering the uncertainties, we can find some small events with stress drop and apparent stress that are quite small. For these events, corner frequencies are estimated to be smaller than expected from cube root scaling and the values for larger events. It is possible that some small events have large stress drop and apparent stress. However, based on these results, which are obtained with the assumption of constant Q, we would conclude that the lower limits of both the stress drop and apparent stress decrease as seismic moment decreases.

[18] This result is essentially the same as the previous result of *Prejean and Ellsworth* [2001]. The only significant difference is the values of Q; the values in this paper are systematically larger than those of *Prejean and Ellsworth* [2001] by a factor about 2. This arises from the difference of the shape of the assumed omega square model. We use a modified version [*Boatwright*, 1978] of the original omega square model [*Brune*, 1970], which was used by *Prejean and Ellsworth* [2001]. We carried out the same analysis for the original model, too. In fact, the residuals and all scaling relationships shown in Figure 3, do not differ significantly between the two models. The reason we used the modified version is that it tends not to create small residuals for a high corner frequency that sometimes results in ambiguity of corner frequency (Figure 2c). We would like to emphasize that the calculated value of Q depends on the model.

[19] Figure 4 shows that there is a strong relationship between stress drop and apparent stress. We find that the ratio of apparent stress to stress drop does not vary with seismic moment. For the omega square spectral model of *Brune* [1970], *Singh and Ordaz* [1994] showed that

$$\sigma_a = 0.23\Delta\sigma_B. \tag{11}$$

If the observed spectra follow equation (1), then the corresponding relation is

$$\sigma_a = 0.33\Delta\sigma_B. \tag{12}$$

We find values that are very close to this line. This result is not surprising because each spectrum is well represented by an omega square model and estimates for the apparent stress to Brune stress drop ratio far from this line would imply a different spectral shape. There are four outliers (events 1, 4, 9, 27). The estimates of P wave energy for these events are higher than those of S wave due to the high values of P wave corner frequency with large errors, and they are unlikely to be reliable. There are many events far from this line in the analysis of *Prejean and Ellsworth* [2001], but that appears to be an artifact of their treating Q estimates differently when calculating the corner frequency and the radiated seismic energy. Specifically, they used single-event estimates of Q when estimating the stress drop and averaged values of Q when estimating apparent stress. In fact, our results indicate that stress drop scales with seismic moment in the same way that the apparent stress does. The same observation might also hold true for the results of *Abercrombie* [1995] when the missing events in her apparent stress estimates [*Ide and Beroza*, 2001] are included.

3. Spectral Ratio Analysis

[20] Though it is frequently used, the validity of a constant Q model is not assured, especially at high frequen-

Table 3. Source Parameter by Spectral Ratio Analysis

ID	M_o^P, N m	M_o^S, N m	f_c^P, Hz	f_c^S, Hz	$\Delta\sigma_B$, MPa
03	1.06e + 11	3.30e + 11	38	25	0.81
12	4.34e + 12	3.93e + 12	16	22	10.4
13	5.34e + 10	5.71e + 10	44	58	2.5
15	1.12e + 12	3.07e + 12	22	13	1.1
18	6.69e + 12	1.85e + 13	12	8.8	2.0
19	4.79e + 11	8.09e + 11	31	24	2.1
20	1.07e + 12	1.84e + 12	21	18	2.0
21	9.37e + 10	1.92e + 11	56	37	1.7
23	1.83e + 11	2.10e + 11	36	41	3.2
24	3.69e + 11	6.43e + 11	41	28	2.6
A1	2.24e + 12	2.18e + 12	21	17	2.6
A2	2.08e + 10	2.14e + 10	95	55	0.83
A3	8.75e + 10	8.57e + 10	55	48	2.3
A4	6.84e + 10	3.47e + 10	87	67	3.7
A5	9.81e + 10	8.95e + 10	40	34	0.87

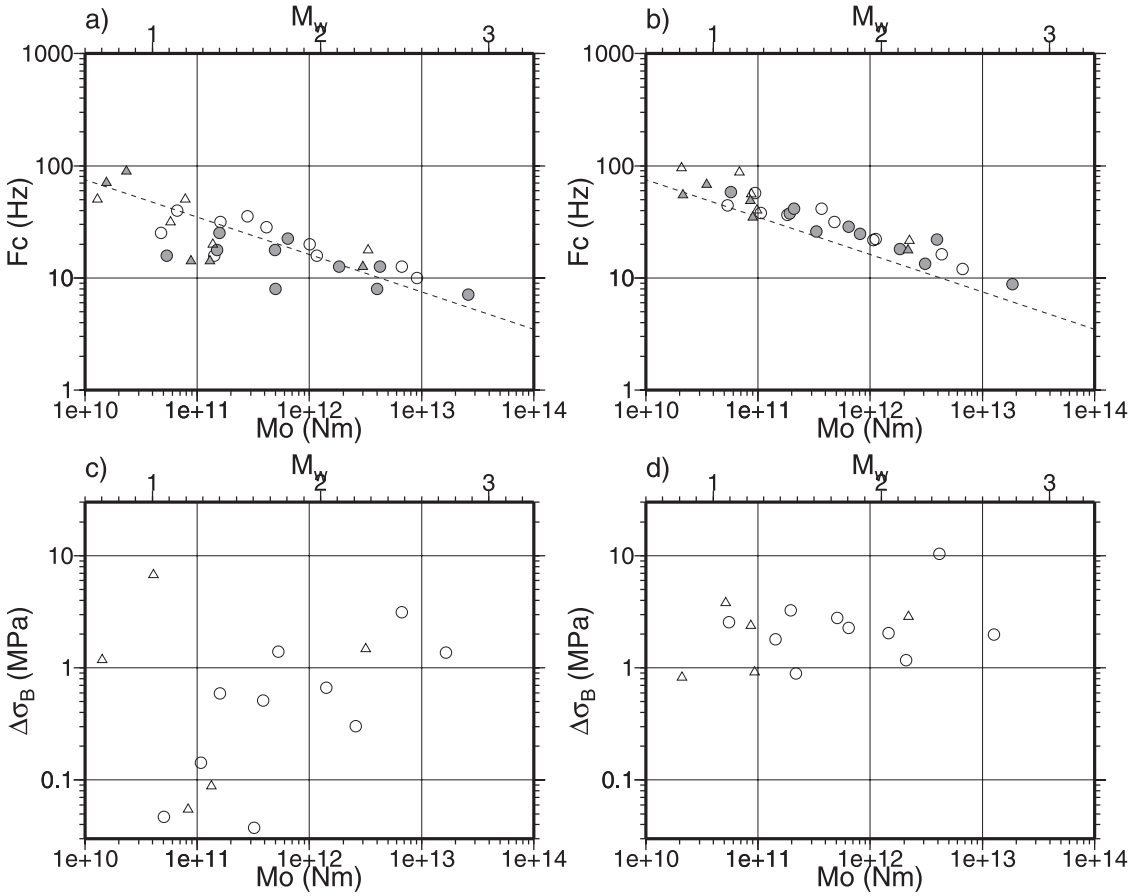

Figure 6. Scaling relations derived from two kind of analyses. (a) Comparison between seismic moment and corner frequency estimated from constant Q analysis. Circle and triangle represent 1997–1998 events (C1) and 1992 events (C2), respectively. Open symbol and gray symbol represent corner frequencies of P and S waves, respectively. (b) Same result as in Figure 6a from spectral ratio analysis. (c) Comparison between seismic moment and Brune stress drop, $\Delta\sigma$, estimated from constant Q analysis. Circle and triangle represent 1997–1998 events (C1) and 1992 events (C2), respectively. (d) Same result as in Figure 6c from spectral ratio analysis.

cies where not much is known about attenuation. However, we can determine the source parameters without assuming path and site effects if we have a set of colocated events [e.g., *Berckhemer*, 1962; *Bakun and Bufe*, 1975; *Mueller*, 1985; *Hough*, 1997]. Using the multiple-empirical Green's function (MEGF) method [*Hough*, 1997] with a slight modification about the assumption on source spectral shape and attenuation behavior, we determine the corner frequencies and relative seismic moments for a cluster of events from 1997 to 1998 located 7 km SE of the borehole and identified as "C1" in Table 1 and another set of events in 1992 (C2). The 10 events in C1 are $1 < M < 3$ and the five events in C2 are $0.5 < M < 2.5$. They show the basic characteristics of size dependencies of stress drop and apparent stress evident in Figure 3.

[21] The ratio between spectra of two events are expressed as

$$\log \dot{u}_k^c(f_i) - \log \dot{u}_l^c(f_i) \approx g\left(f_i; \log M_{ok}, 1/Q^c, f_{ck}^c\right) - g\left(f; \log M_{ol}, 1/Q^c, f_{cl}^c\right). \quad (13)$$

If the path is common to the two spectra, the right hand side of the above equation can be written as

$$\log M_{ok} - \log M_{ol} + \frac{1}{2} \log \frac{\left(1 + \left(f_i/f_{cl}^c\right)^4\right)}{\left(1 + \left(f_i/f_{ck}^c\right)^4\right)}. \quad (14)$$

and the unmodeled effects of attenuation are removed from the problem.

[22] When there are N points of frequency data for each spectra and M events, we have $N * M(M-1)/2$ equations to determine M seismic moments and M corner frequencies. However, these equations do not supply information about the absolute values of seismic moments. We add another equation to equalize the logarithmic average of seismic moments to that determined by the previous constant Q analysis for events in the C1 cluster.

[23] These $N * M(M-1)/2 + 1$ equations are solved by nonlinear inversion using the Levenberg-Marquart method. In such a nonlinear inversion it can be difficult to find a global minimum solution; however, as shown in the constant Q

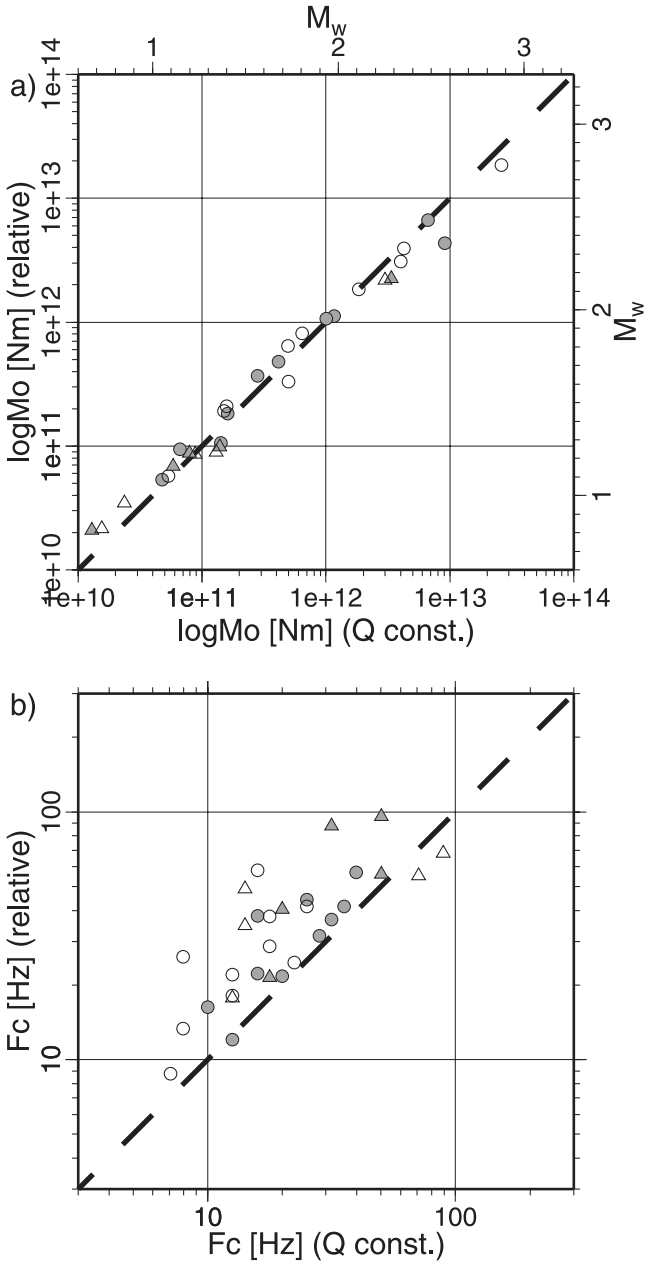

Figure 7. Comparison between (a) seismic moment and (b)corner frequency estimated from constant Q analysis and spectral ratio analysis. Circle and triangle represent 1997–1998 events (C1) and 1992 events (C2), respectively. Open symbol and gray symbol represent parameters of P and S waves, respectively.

analysis, the residual changes gradually with corner frequency (Figure 2). This means that the nonlinearity is weak and that our linearized method should readily converge to the global minimum. We solved the system from an extreme initial condition in which all seismic moments are the average moment value and all corner frequencies are 10 Hz.

[24] In our analysis we have 10 events and 45 spectral ratio curves for C1 and five events and 10 curves for C2, for both P and S waves. Some of these curves are shown in Figure 5 together with the best fitting model. Table 3 summarizes the estimated parameters and the values of stress drop calculated from these values using equations (9). Figure 5 suggests that the corner frequencies for EV13, EV21, and EVA2 may not be well resolved since the upper limit of analysis range is close and there is little flat part of spectral ratio. That the corner frequencies of these events are near the upper limit of our observation band means that we can only place a lower bound on the corner frequencies. Thus, if anything, the stress drops of these very small events are higher than we estimate.

[25] Figure 6 compares the estimated corner frequencies and stress drops to the seismic moments. The corner frequencies follow cube root scaling with seismic moment and a 1 MPa stress drop (Figure 6b), while those of constant Q analysis tend to be small for small events (Figure 6a). The stress drops show almost no size dependence and are generally higher than 1 MPa (Figure 6d), which is substantially higher than the stress drops found from the constant Q analysis of the same events (Figure 6c). This difference arises from the difference in estimates of the corner fre-

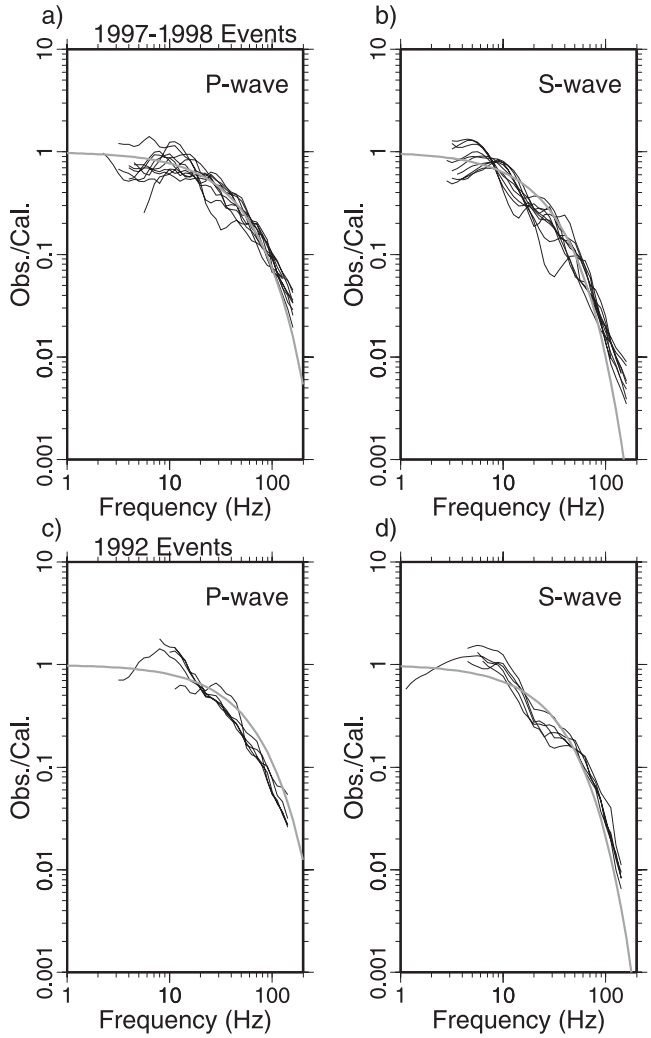

Figure 8. Ratios between observed and calculated spectra (black line) using parameters determined by spectral ratio analysis for (a) P or (b) S waves for C1 cluster and (c) P or (d) S waves for C2 cluster. Gray line is the attenuation curve for the case of Q = 150.

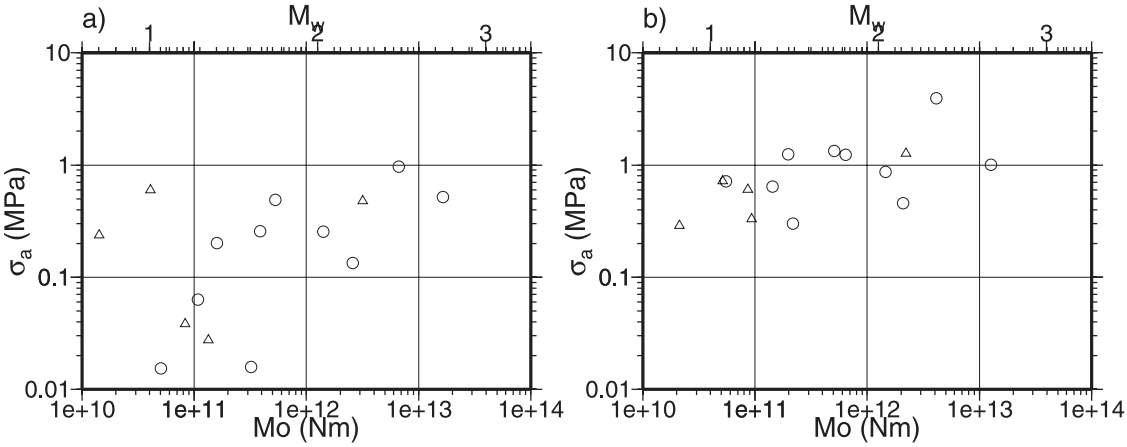

Figure 9. Comparison between seismic moment and apparent stress in constant Q analysis and spectral ratio analysis. Circle and triangle represent 1997–1998 events (C1) and 1992 events (C2), respectively.

quencies (Figure 7). Estimated seismic moments from the two methods are consistent. For some events, the difference in corner frequency between the two analyses is more than a factor of two, which results in a difference of more than an order of magnitude in the stress drop.

4. Discussion

[26] We have shown how two different methods for recovering source properties can give very different results. The cause of the difference may be a propagation effect that can affect source estimates even in the relatively clean recording environment of a deep borehole. Using the set of estimated parameters, we can investigate what attenuation behavior is required to explain the differing results. By taking the ratio between observed and calculated spectra, we can derive attenuation curves for P and S waves for two groups of events (Figure 8). Except for low frequencies where the noise is large, the curves all have similar forms in every figure. At frequencies between 30 and 100 Hz, these curves are well explained by a constant Q model of $Q = 150$ for all cases. However, we can see departure from these curves at higher and lower frequencies. The attenuation is not as high as predicted by $Q = 150$ over 100 Hz for the C1 group. The attenuation is also small around 8–10 Hz, so amplification is required to explain the bump. On the other hand, stronger attenuation exists at around 20 Hz, to particularly for the S waves.

[27] The behavior between 5 and 100 Hz is common for both groups, which suggests that this is not an instrumental effect. This kind of frequency dependent amplification/attenuation is not usually expected for deep borehole observation. One possible explanation is that the sensor is only about 25 m below the contact between the precaldera basement rocks and the overlying tuff. We cannot separate reflection or backscattering from this boundary from the direct arrival, so this effect might create a complex path/site effect. The difference of the behavior above 100 Hz might be an instrumental effect or arise from the difference in path between the two clusters. Since the location of the C2 cluster is just 1 km closer to the borehole and 1 km shallower than cluster C1, the path of C2 is not much different from that of C1. However, the wavelength is about 30–50 m at a frequency of 100 Hz, so the different locations could have an important effect.

[28] By assuming that the path and site effects are given by the logarithmic average of these attenuation curves, $A^c(f)$, we can calculate the radiated energy and apparent stress (Figure 9, Table 4) using

$$E^c = 4\pi\rho v^c r^2 \times 2 \int_{f_0}^{f_1} \left| \frac{\dot{u}^c(f)}{A^c(f)} \right|^2 df \qquad (15)$$

and equation (8). In this calculation we added missing energy above 180 Hz by extrapolation of the omega square model [*Ide and Beroza*, 2001]. Again, there is little size dependence in apparent stress. In fact, the estimates for EV13, EV21, and EVA1 are the lower limit of apparent stress since the upper limit is close to the corner frequency. Nevertheless, these values are much higher than the estimates of constant Q analysis. The smallest value is 0.3 MPa, which is more than 10 times larger than the estimate from the constant Q analysis.

[29] Figure 10 illustrates why such a large difference in apparent stress arises using EV13, the event with the largest difference. Though $Q = 150$ is a good average of overall attenuation as shown in Figure 8, small values of Q produce

Table 4. Energy and Apparent Stress by Spectral Ratio Analysis

ID	$\bar{M}_o$, N m	$\bar{E}^P + \bar{E}^S$, J	σ_a, MPa
03	2.18e + 11	2.43e + 06	0.33
12	4.14e + 12	6.04e + 08	4.3
13	5.52e + 10	1.46e + 06	0.78
15	2.10e + 12	3.56e + 07	0.50
18	1.26e + 13	4.71e + 08	1.1
19	6.44e + 11	2.95e + 07	1.3
20	1.46e + 12	4.68e + 07	0.94
21	1.43e + 11	3.38e + 06	0.69
23	1.96e + 11	9.04e + 06	1.4
24	5.06e + 11	2.50e + 07	1.5
A1	2.21e + 12	1.04e + 08	1.4
A2	2.11e + 10	2.26e + 05	0.31
A3	8.66e + 10	1.94e + 06	0.66
A4	5.16e + 10	1.37e + 06	0.78
A5	9.38e + 10	1.15e + 06	0.36

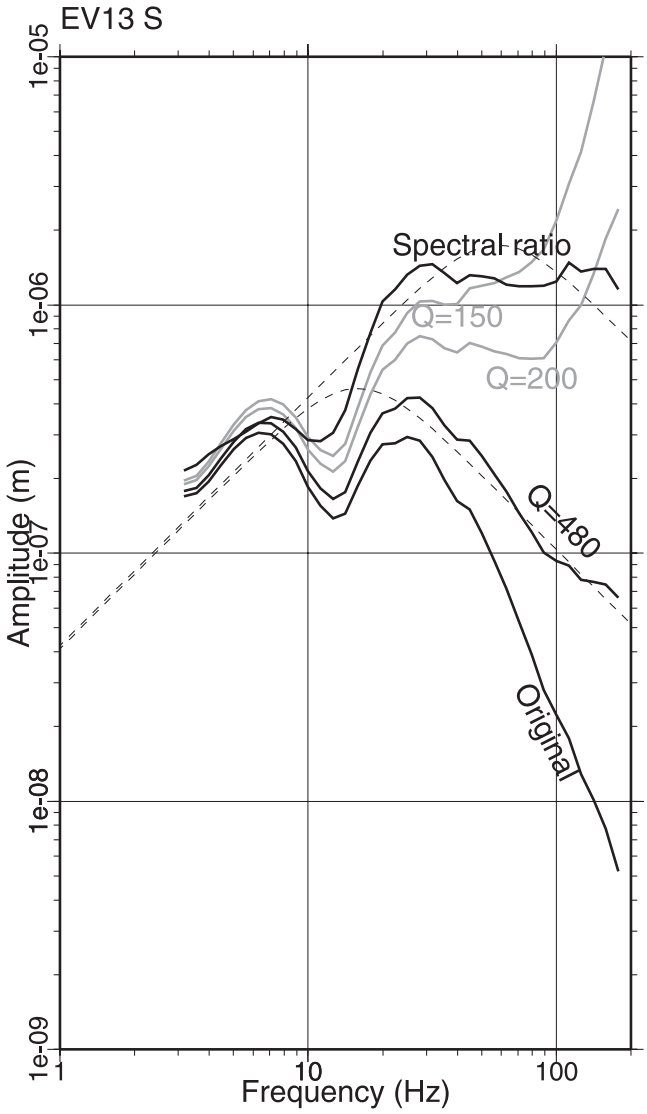

Figure 10. Difference of velocity spectrum used to calculate radiated energy. Solid lines are original spectrum, constant Q (=480) corrected one, and that with site and path correction based on spectral ratio analysis. Dashed lines are fitted omega square model for constant Q analysis and spectral ratio analysis. Gray line is an example of smaller Q (=150).

anonymously large amplitude for frequencies higher than 100 Hz. Hence we get a solution at $Q = 480$ for constant Q analysis. When we use the average attenuation curves obtained by spectral ratio analysis, the modeled spectrum has a higher corner frequency. Since the energy is given as an integral over frequency, the discrepancy at high frequency is more significant. The difference shown in Figure 10 corresponds to a factor of 50 in seismic energy. For most events of the clusters C1 and C2, the estimated values of Q are larger than 150, and this is the explanation for overall underestimation of energy by constant Q analysis.

[30] The values of apparent stress are comparable to previous estimates for larger earthquakes [e.g., *Kanamori et al.*, 1993; *Mayeda and Walter*, 1996]. Though there are no estimates of energy in the MEGF study of small events ($0 < M < 1.5$) by *Hough et al.* [1999], most events have stress drops larger than 1 MPa, which are consistent with our estimates since there is a strong relationship, $\sigma_a = 0.33\Delta\sigma_B$ (Figure 4).

[31] Many previous studies have reported a size dependence of stress drop even after correction for constant Q [e.g., *Masuda and Suzuki*, 1982; *Fletcher and Boatwright*, 1991]. Such size dependence is observed for surface observations and is usually explained by attenuation, especially site-controlled $f_{\max}$ [*Hanks*, 1982]. Our results indicate that frequency dependent amplification and attenuation should be considered even for borehole observations.

[32] Seismograms for two of the events in the C1 cluster (IDs 20 and 23) appear in Figure 4 (displacement) and Figure 5 (velocity) of *Prejean and Ellsworth* [2001]. The recordings display well-developed coda waves in the wake of the body wave arrivals, indicating that the homogeneous whole space assumption contained in (1) and used in the spectral method is not entirely justified. Indeed, it would be more appropriate to include in (1) either a frequency dependent "path" amplitude factor or frequency dependent Q, or both. While these factors cancel in the MEGF method, we ultimately want to be able to interpret borehole seismograms in the time domain, for which new approaches may be required.

5. Conclusions

[33] The scaling relations of earthquake stress drop and apparent stress are sensitive to wave propagation effects and can be affected by an artificial size dependency if it is not properly modeled. We reexamined the data of *Prejean and Ellsworth* [2001] from a 2-km-deep borehole in Long Valley Caldera, California. First, assuming an omega square model with a constant Q, we determined the stress drop and apparent stress of 46 events ($0.5 < M_w < 5.0$). We find that some small events have small apparent stresses of about 0.003–0.03 MPa, and also find that these events have low stress drops of 0.01 to 0.1 MPa. Most larger events have both larger stress drops of 1–10 MPa and larger apparent stresses. This analysis supports the decrease of apparent stress with decreasing moment.

[34] We expect that the Brune stress drop would have a strong relationship to the apparent stress. We find that an omega square model where $\sigma_a = 0.33\Delta\sigma_B$ fits our data well. Insofar as no systematic change in the spectral shape is observed with seismic moment in the data, it is unlikely that stress drop and apparent stress will have different dependencies on seismic moment.

[35] We also estimated stress drops using spectral amplitude ratios for 15 colocated events ($1 < M_w < 3$) of two clusters. In this case we assumed an omega square model, but relied on spectral ratios to eliminate the effects of attenuation. We found that the shape of the spectral ratios are consistent with an omega square model; however, the corner frequencies measured using spectral ratios are significantly higher for small events than the corner frequencies measured by fitting spectra. We believe the spectral ratio measurements are more reliable because they account for propagation effects and make no assumption about the frequency dependence of attenuation. These more reliable measurements follow constant stress drop and constant apparent stress scaling.

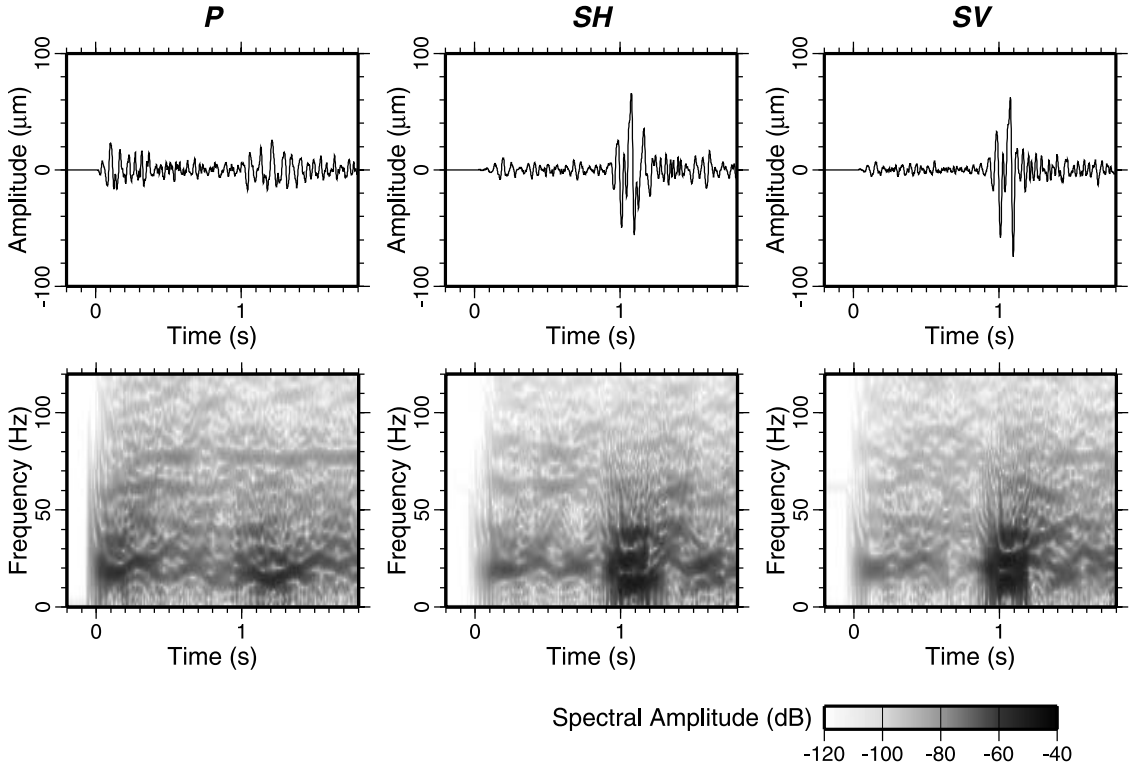

Figure A1. Example of spectrogram calculated for rotated waveforms (*P*, *SH*, and *SV*) of EV20. Each spectral amplitude is calculated using 0.2 s time window with 10% cosine taper at 0.01 s time interval.

[36] The difference in the two results demonstrate how propagation effects and/or a constant Q assumption can introduce an artificial size dependence in apparent stress measurements. Our observations can be reconciled if the body wave spectrum assumed in equation (1) is reshaped by propagation through a nonconstant Q medium and/or by purely elastic path or site effects. Although such amplification and/or attenuation behavior has not previously been considered for borehole observations in basement rock, results from the MEGF method suggest that they may be important. Thus previous measurements of the scaling of small earthquake source parameters derived from borehole observations may need to be reevaluated.

Appendix A: Coda Waves and Length of Time Window

[37] Ideally, we should use only direct waves in the formulation of equation (1), considering Q as a total effect of intrinsic and scattering attenuation. However, this cannot be satisfied in a natural environment and there are coda waves arriving from almost the same time as direct waves

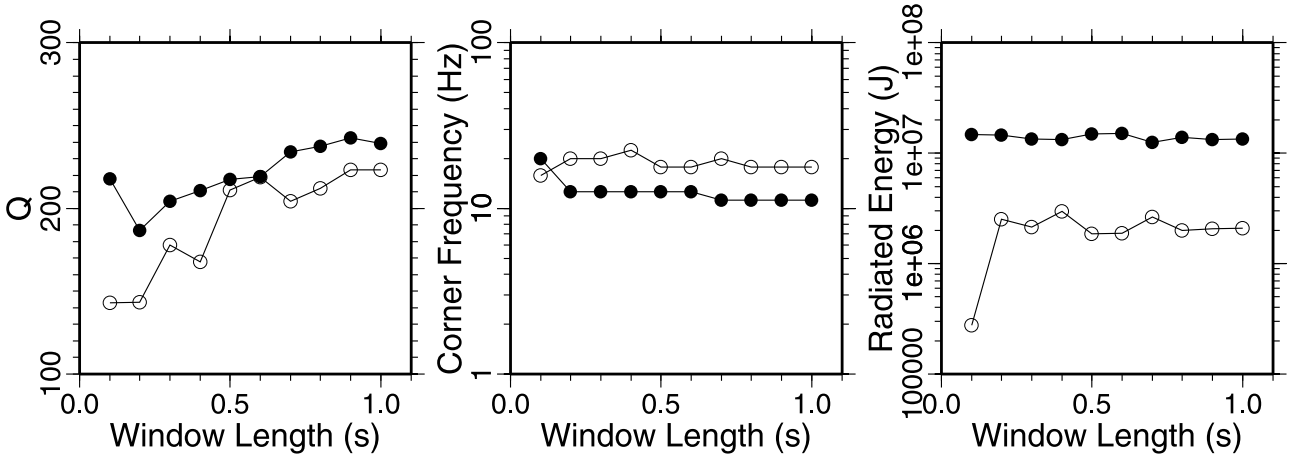

Figure A2. Difference of parameters in constant Q analysis for different time window. Windows are taken from just after wave arrival. Event is EV20, same as Figure A1. Open and solid circles represent *P* and *S* waves, respectively.

and these waves are inseparable from the direct waves. It is important to recognize this and to consider its effect on parameter estimation.

[38] Figure A1 shows an example of spectrograms calculated for EV20. We see large amplitude of direct *P* and *S* arrivals that are strongest around 20 Hz. Waves of about 60 Hz and 75 Hz arrive later by about 0.1–0.2 s than these direct wave arrivals. These waves are probably scattered waves and including these waves can affect the resulting parameters.

[39] Fortunately, the results depend only slightly on the choice of time window showing that the effect of coda waves is not significant for most events. Figure A2 shows the difference of parameters determined using different time window length. Q increases as window length increases. However, for windows longer than 0.5 s, the difference is small. Moreover, corner frequencies and energies are less sensitive. This is because corner frequencies are determined mostly by direct waves around the arrival times and because each spectrum is modified to be similar to a common omega square model by different Q value for each window length before integration for the energy calculation.

[40] In the spectral ratio analysis, we should use the same window length to include the same direct and scattered waves. Strictly speaking, this is not possible because a larger event has a longer source duration and requires a longer time window. Using a longer window will include more common propagation effects; however, the meaning of Q is clearer for the shorter window. The choice of 0.4 s for the *P* window and 0.6 s for the *S* window in this study is a compromise between these two considerations. We have tested other values and obtained similar results, both for the constant Q analysis and the spectral ratio analysis.

[41] **Acknowledgments.** We thank Phil Harben, Don Rock, and Paul Kasameyer of Lawrence Livermore National Laboratory for installation of their borehole seismometer and Reftek recording system in the 1992 and 1997–1998 experiments. We also thanks Hisao Ito and Takao Ohminato of the Geological Survey of Japan for installation of their Kinkei recording system. Peter Malin of Duke University and Stuart Wilkinson of the USGS provided invaluable assistance in the field. We thank Sue Hough, Arthur McGarr, Shri Krishna Singh, and Ralph Archuleta for helpful reviews. Kazutoshi Imanishi and Anna Stork helped us to investigate the difference of omega square model assumption. S.I was supported by Grant-in-Aid for Scientific Research of the Ministry of Education, Sports, Science and Technology. G.C.B. was supported by NSF grant EAR-0208499.

References

Abercrombie, R. E., Earthquake source scaling relationships from −1 to 5 M_L using seismograms recorded at 2.5-km depth, *J. Geophys. Res.*, *100*, 24,015–24,036, 1995.

Abercrombie, R. E., A summary of attenuation measurements from borehole recordings of earthquakes: The 10 Hz transition problem, *Pure Appl. Geophys.*, *153*, 475–487, 1998.

Aki, K., Scaling law of seismic spectrum, *J. Geophys. Res.*, *72*, 1217–1231, 1967.

Aki, K., and P. Richards, *Quantitative Seismology*, 932 pp., W. H. Freeman, New York, 1980.

Anderson, J. G., and J. R. Humphrey Jr., A least squares method for objective determination of earthquake source parameters, *Seismol. Res. Lett.*, *62*, 201–209, 1991.

Archuleta, R. J., Downhole recordings of seismic radiation, in *Earthquake Source Mechanics*, *Geophys. Monogr. Ser.*, vol. 37, edited by C. H. Scholz, pp. 311–318, AGU, Washington, D. C., 1986.

Archuleta, R. J., E. Cranswick, C. Mueller, and P. Spudich, Source parameters of the 1980 Mammoth Lakes, California, earthquake sequence, *J. Geophys. Res.*, *87*, 4595–4607, 1982.

Bakun, W. H., and C. G. Bufe, Shear-wave attenuation along the San Andreas fault zone in central California, *Bull. Seismol. Soc. Am.*, *65*, 439–459, 1975.

Berckhemer, H., Die ausdehnung der Bruchfläche im Erdbeben herd und ihr Einfluss auf das seismische Wellen spektrum, *Gerlands Beitr. Geophys*, *71*, 5–26, 1962.

Boatwright, J., Detailed spectral analysis of two small New York State earthquakes, *Bull. Seismol. Soc. Am.*, *68*, 1131–1177, 1978.

Boatwright, J., and J. B. Fletcher, The partition of radiated energy between *P* and *S* waves, *Bull. Seismol. Soc. Am.*, *74*, 361–376, 1984.

Boore, D. M., The effect of finite bandwidth on seismic scaling relationships, in *Earthquake Source Mechanics*, *Geophys. Monogr. Ser.*, vol. 37, edited by C. H. Scholz, pp. 275–283, AGU, Washington, D. C., 1986.

Brune, J. N., Tectonic stress and spectra of seismic shear waves from earthquakes, *J. Geophys. Res.*, *75*, 4997–5009, 1970. (Correction, *J. Geophys. Res.*, *76*, 5002, 1971.)

Di, M., and A. Rovelli, Effects of the bandwidth limitation on stress drops estimated from integrals of the ground motion, *Bull. Seismol. Soc. Am.*, *78*, 1818–1825, 1988.

Fletcher, J. B., and J. Boatwright, Source parameters of Loma-Prieta aftershocks and wave-propagation characteristics along the San-Francisco Peninsula from a joint inversion of digital seismograms, *Bull. Seismol. Soc. Am.*, *81*, 1783–1812, 1991.

Gibowicz, S. J., R. P. Young, S. Talebi, and D. J. Rawlence, Source parameters of seismic events at the Underground Research Laboratory in Manitoba, Canada: Scaling relations for events with moment magnitude smaller than −2, *Bull. Seismol. Soc. Am.*, *81*, 1157–1182, 1991.

Hanks, T. C., Earthquake stress drops, ambient tectonic stresses and stresses that derive plate motions, *Pure Appl. Geophys.*, *115*, 441–458, 1977.

Hanks, T. C., f_{max}, *Bull. Seismol. Soc. Am.*, *72*, 1867–1880, 1982.

Hough, S. E., Observational constraints on earthquake source scaling: Understanding the limits in resolution, *Tectonophysics*, *261*, 83–96, 1996.

Hough, S. E., Empirical Green's function analysis: Taking the next step, *J. Geophys. Res.*, *102*, 5369–5384, 1997.

Hough, S. E., J. M. Lees, and F. Monastero, Attenuation and source properties at the Coso Geothermal area, California, *Bull. Seismol. Soc. Am.*, *89*, 1606–1609, 1999.

Ide, S., and G. C. Beroza, Does apparent stress vary with earthquake size?, *Geophys. Res. Lett.*, *28*, 3349–3352, 2001.

Jost, M. L., T. Büßelberg, Ö. Jost, and H.-P. Harjes, Source parameters of injection-induced microearthquakes at 9 km depth at the KTB deep drilling site, Germany, *Bull. Seismol. Soc. Am.*, *88*, 815–832, 1998.

Kanamori, H., and D. L. Anderson, Theoretical basis of some empirical relations in seismology, *Bull. Seismol. Soc. Am.*, *65*, 1073–1095, 1975.

Kanamori, H., E. Hauksson, L. K. Hutton, and L. M. Jones, Determination of earthquake energy release and M_L using TERRAscope, *Bull. Seismol. Soc. Am.*, *83*, 330–346, 1993.

Masuda, T., and Z. Suzuki, Objective estimation of source parameters and local Q values by simultaneous inversion method, *Phys. Earth Planet. Inter.*, *30*, 197–208, 1982.

Mayeda, K., and W. R. Walter, Moment, energy, stress drop, and source spectra of western U.S. earthquakes from regional coda envelopes, *J. Geophys. Res.*, *101*, 11,195–11,208, 1996.

McGarr, A., On relating apparent stress to the stress causing earthquake fault slip, *J. Geophys. Res.*, *104*, 3003–3011, 1999.

Mueller, C. S., Source pulse enhancement by deconvolution of an empirical Green's function, *Geophys. Res. Lett.*, *12*, 33–36, 1985.

Prejean, S. G., and W. L. Ellsworth, Observations of earthquake source parameters and attenuation at 2 km depth in the Long Valley Caldera, eastern California, *Bull. Seismol. Soc. Am.*, *91*, 165–177, 2001.

Singh, S. K., and M. Ordaz, Seismic energy release in Mexican subduction zone earthquakes, *Bull. Seismol. Soc. Am.*, *84*, 1533–1550, 1994.

Waldhauser, F., and W. L. Ellsworth, A double-difference earthquake location algorithm: Method and application to the northern Hayward fault, California, *Bull. Seismol. Soc. Am.*, *90*, 1353–1368, 2000.

Wyss, M., and J. N. Brune, Seismic moment, stress, and source dimensions for earthquakes in the California-Nevada region, *J. Geophys. Res.*, *73*, 4681–4694, 1968.

G. C. Beroza, Department of Geophysics, Stanford University, 397 Panama Mall, Stanford, CA 94305-2215, USA. (beroza@pangea.stanford.edu)

W. L. Ellsworth and S. G. Prejean, U.S. Geological Survey, 345 Middlefield Road, Menlo Park, CA 94025, USA. (ellsworth@usgs.gov; sprejean@usgs.gov)

S. Ide, Department of Earth and Planetary Science, University of Tokyo, 7-3-1 Hongo, Bunkyo, Tokyo, 113-0033, Japan. (ide@eps.s.u-tokyo.ac.jp)